Supporting Information

Lifetime-Encoded Infrared-Emitting Nanoparticles for *in Vivo* Multiplexed Imaging

Dirk H. Ortgies[†ϸΔ], Meiling Tan[‡Δ], Erving C. Ximendes[ɪΔ], Blanca del Rosal[ϙ], Jie Hu[†], Lei Xu[‡], Xindong Wang[‡], Emma Martín Rodríguez[&ϸ], Carlos Jacinto[ɪ], Nuria Fernandez[⊐ϸ], Guanying Chen[‡]* and Daniel Jaque[†ϸ]*

† Fluorescence Imaging Group, Departamento de Física de Materiales, Universidad Autónoma de Madrid, Madrid 28049, Spain

‡ MIIT Key Laboratory of Critical Materials Technology for New Energy Conversion and Storage, School of Chemistry and Chemical Engineering & Key Laboratory of Micro-systems and Micro-structures, Ministry of Education, Harbin Institute of Technology, 150001 Harbin, People's Republic of China.

ɪ Grupo de Fotônica e Fluidos Complexos, Instituto de Física, Universidade Federal de Alagoas, 57072-900 Maceió-AL, Brazil

& Fluorescence Imaging Group, Departamento de Física Aplicada, Universidad Autónoma de Madrid, Madrid 28049, Spain

⊐ Fluorescence Imaging Group, Departamento de Fisiología, Facultad de Medicina, Avda. Arzobispo Morcillo 2, Universidad Autónoma de Madrid, 28029 Madrid, Spain.

ϙ Centre for Micro-Photonics, Faculty of Science, Engineering and Technology, Swinburne University of Technology, PO Box 218, Hawthorn, VIC 3122, Australia

ϸ Nanobiology Group, Instituto Ramón y Cajal de Investigación Sanitaria, IRYCIS, Ctra. Colmenar km. 9.100, Madrid 28034, Spain.

[Δ] These authors contributed equally

S1.- Time domain analysis of fluorescence images.

Fluorescence lifetime images (FLIM) are produced by acquiring a series of time-gated fluorescence intensity images at a range of time delays after excitation (**Figure S1(a)** and **(b)**) and, for each pixel in the field of view, fitting the decay profile to an assumed model. According to the literature, the most suitable model is the one defined by the stretched exponential function (StrEF), also known as the Kohlrausch-Williams-Watts function, expressed as (see **Figure S1(c)**):[1,2]

$$I(t) = I_0 \exp\left(-\left(\frac{t}{\tau_k}\right)^{\beta}\right) \quad \text{(S1)}$$

where I_0 is the initial intensity at t = 0, τ_k the characteristic time constant and β the heterogeneity parameter ($0 < \beta < 1$). The smaller the value of β is, the broader is the distribution of fluorescence lifetimes within a sample, *i.e.* the higher its heterogeneity. In the special case of $\beta = 1$ (minimal heterogeneity) StrEF becomes a single exponential. As one can see, the StrEF is much more appropriate to describe the decay in heterogeneous tissue samples showing continuous lifetime distributions than multi-exponential models with an arbitrary number of discrete lifetimes (which could just as well vary from pixel to pixel). Hence, the computational cost is significantly reduced.

However, in order to correctly describe the decay, it is necessary to interpret the lifetimes in a statistical manner (notice that τ_k in **Equation S1** is purposefully defined as the characteristic time constant and not the characteristic lifetime). The possibility that we explored was the so called 95-percentile lifetime, *i.e.*, the mean lifetime $<\tau>$ of the distribution as obtained from the integration of Equation S1:[3]

$$<\tau> = \frac{1}{\beta}\,\tau_k \Gamma\left(\frac{1}{\beta}\right) \quad \text{(S2)}$$

where Γ is the gamma function.

Once the values of $<\tau>$ and I_0 were obtained, two different images were created: the first having $<\tau>$ determining the value of pixels and the second having I_0. The first image received a pseudo coloring treatment (the color scale was suitably chosen to point out the contrast between lifetimes) while the second remained a black and white picture. Having those two images, we multiplied them to produce the final fluorescence lifetime image (**Figure S1(d)**). By multiplying those images, it was ensured that the brightest points on the FLIM were the ones having higher emission.

The lifetime resolution of our system is limited by the camera speed and background noise, by the rise/fall time of the diode laser and by the finesse of the fitting protocol in our analyzing software. With the experimental set-up here available in our laboratory, we estimate that the lifetime resolution is ± 20 μs being this limited by the uncertainty of the fitting procedure. Therefore nanoparticles with lifetime differences well in excess of 20 μs should be employed. Regarding the spatial resolution, this can be assumed to be the same of intensity-based fluorescence images that is estimated to be better than 1 mm. The future improvement of both temporal and spatial resolution would imply the use of faster cameras and laser diodes and larger magnification optics.

.

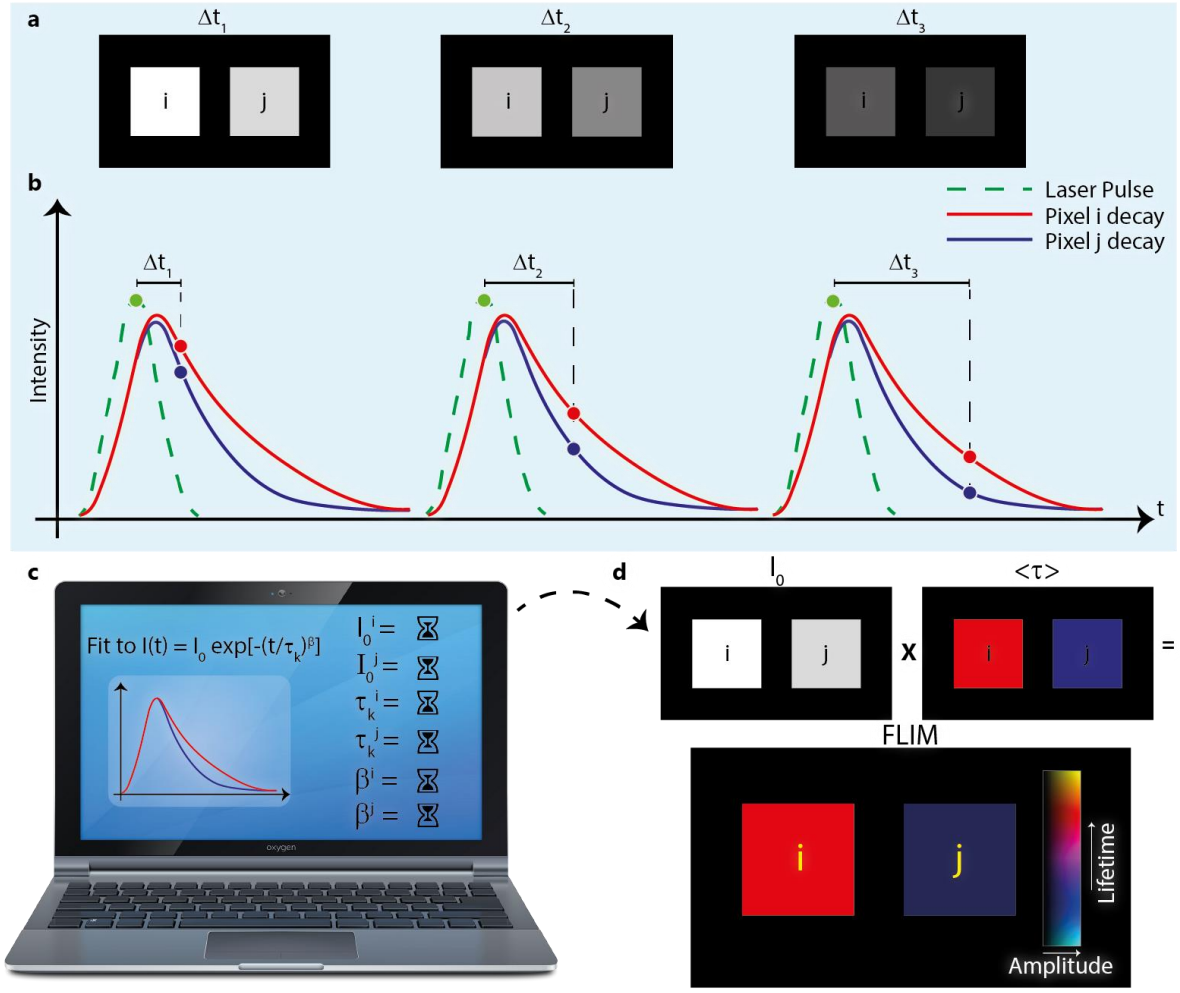

Figure S1.1. **(a)** Series of time-gated fluorescence intensity images. **(b)** Acquisition process. For each fluorescence image obtained at Δt_x, a new point of the decay profile of every pixel is added to the analysis. **(c)** Schematic representation of the computational fitting process to the stretched exponential function. **(d)** Multiplication between the amplitude image (black and white) and lifetime map (colorful) in order to produce the final fluorescence lifetime image.

Figure S1.2 includes, as an illustrative example, both the intensity and lifetime-based images of four Eppendorf tubes containing colloidal solutions of $NaY_{0.9-x}Yb_{0.1}Nd_xF_4@CaF_2$ NPs with a Nd contents of x = 0.1, 0.2, 0.3 and 0.5. Note that due to their very different fluorescence lifetimes these samples give very different colors in the lifetime-based image.

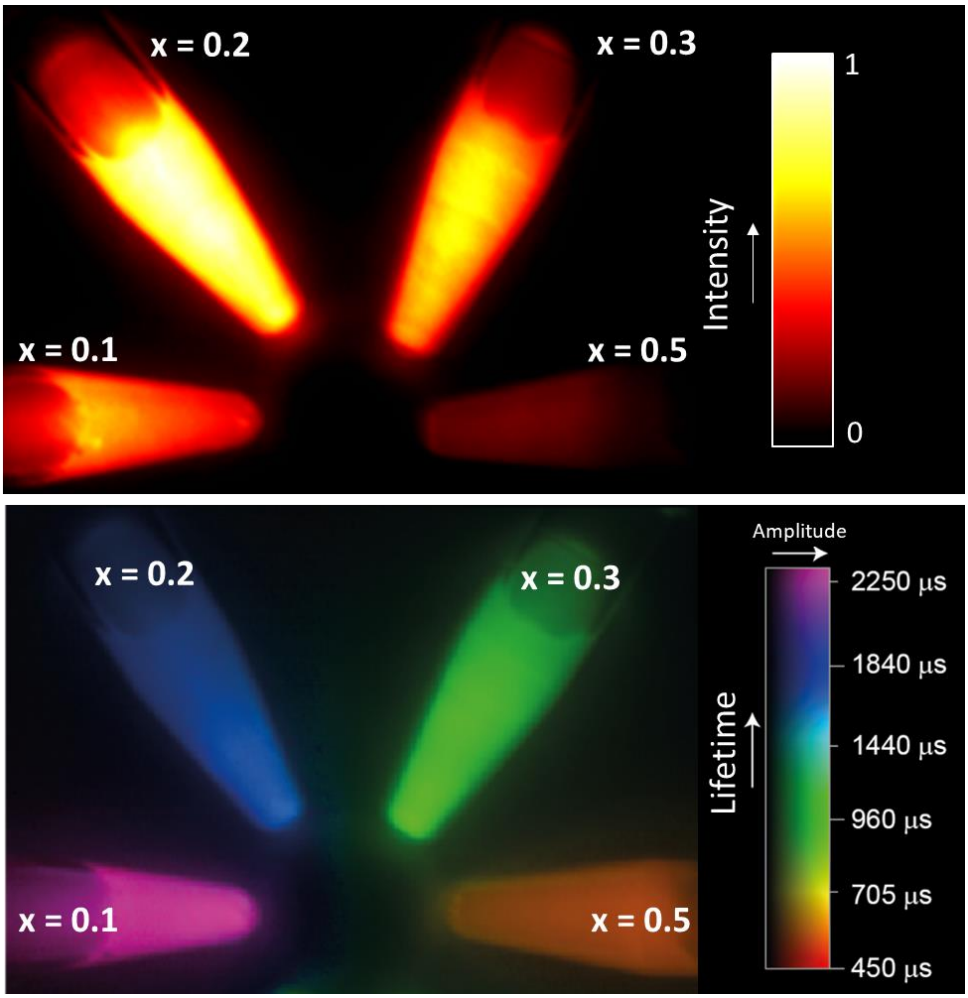

Figure S1.2 Intensity (top) and lifetime-based (bottom) images of four Eppendorf tubes containing colloidal solutions of $NaY_{0.9-x}Yb_{0.1}Nd_xF_4@CaF_2$ NPs with Nd^{3+} contents of x = 0.1, 0.2, 0.3 and 0.5.

In order to discuss the time resolution and speed of our experimental system we measured the time response of both laser diode and delayer circuit. To measure the laser diode switch–off time (that is the one relevant in our measurements) we used a 10 ns response photodiode to measure the laser tail. Results are shown in **Figure S1.3 (a)**. As can be observed, our laser diode shows a fall time close to 5 µs whereas the delay circuit presents a faster response with a rise/fall time of 45 ns (see **Figure S1.3 (b)**). At this point we would like to highlight that the response time of the CCD camera can also play a role in the performance of our system. In particular, the reading time required by the camera to provide an image would determine the resolution in our lifetime measurements. After consulting the camera manufacturer, we could not get an exact value for this time. Nevertheless, the minimum

integration time that the software allows to set was 10 µs. This is here interpreted as the minimum time required by the CCD detector for image acquisition plus the time required for information transfer to software and subsequent image formation. Thus, taking into account the fall time of the laser diode and the time required by camera to build up the fluorescence image we concluded that the time resolution of our time gating system is ± 15 µs.

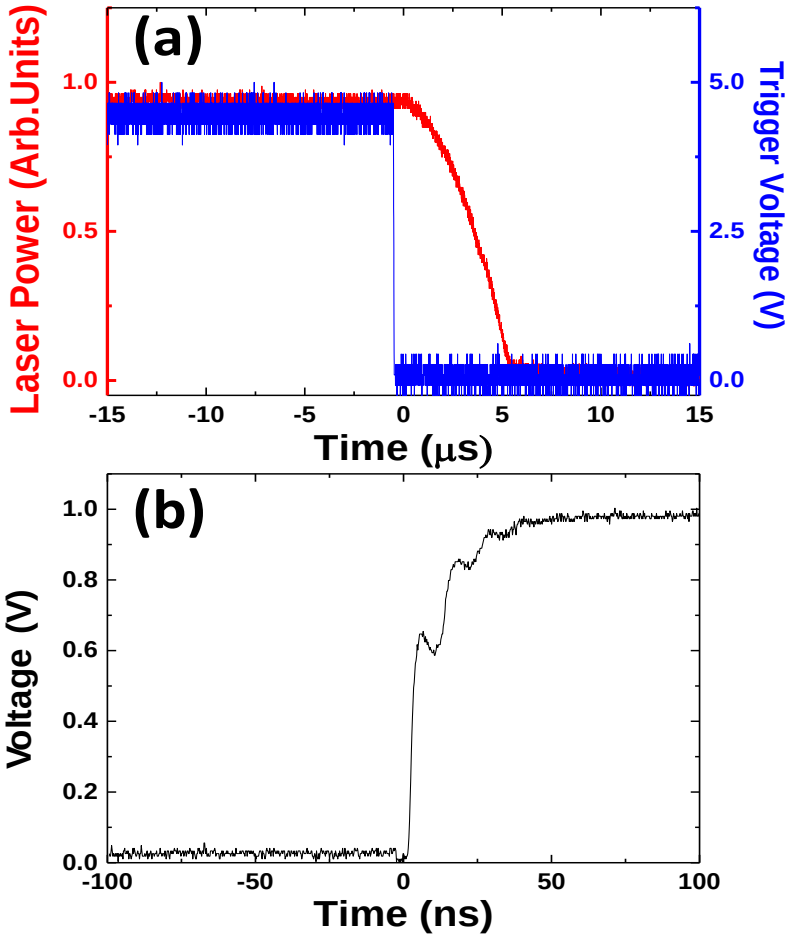

Figure S1.3. (a) Time evolution of the laser intensity after being switched off (red line). The time evolution of the trigger pulse is also included (blue line). A fall time of 5 µs for our excitation source is estimated. **(b)** Time evolution of trigger pulse generated by the delayer circuit, showing a rise/fall time of 45 ns.

S2 Morphological characterization of $NaYF_4$:Yb,Nd @CaF_2 core/shell nanoparticles.

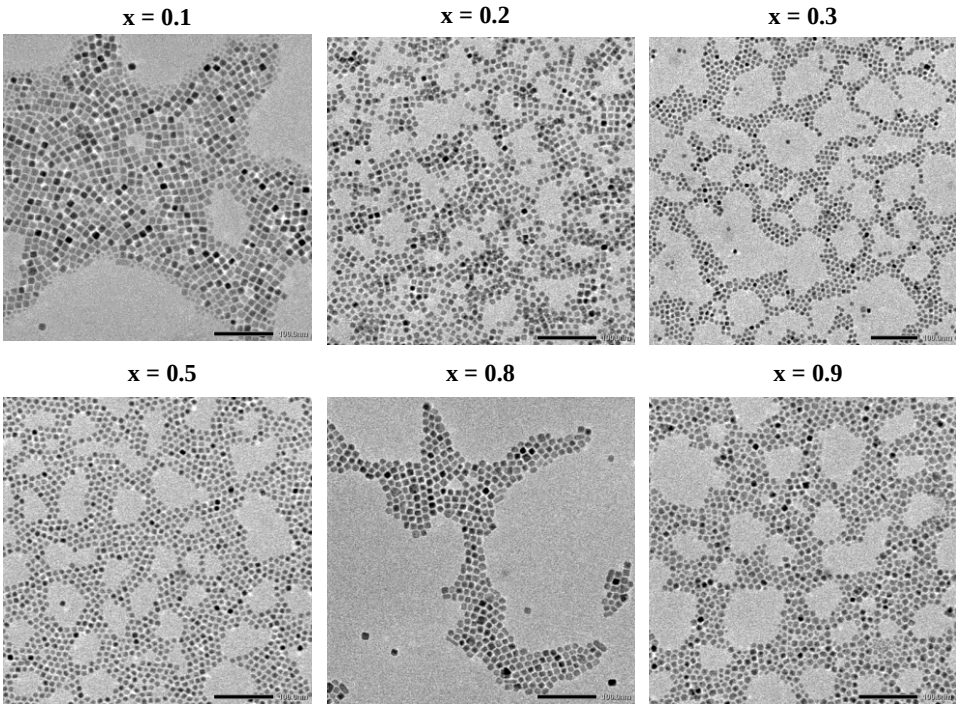

Figure S2.1. TEM images of the $NaY_{0.9-x}Yb_{0.1}Nd_xF_4$@$CaF_2$ core/shell NPs with different Nd^{3+} doping concentrations. Scale bar is 100 nm.

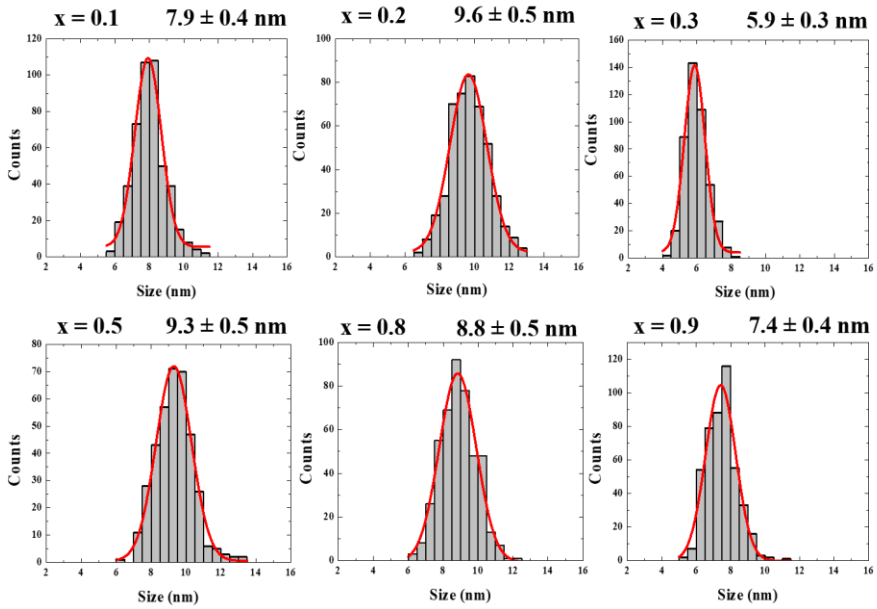

Figure S2.2. Size histogram corresponding to the $NaY_{0.9-x}Yb_{0.1}Nd_xF_4$@$CaF_2$ core/shell NPs with different Nd^{3+} doping levels. Data obtained from the statistical analysis of the images is included in Figure S2.2.

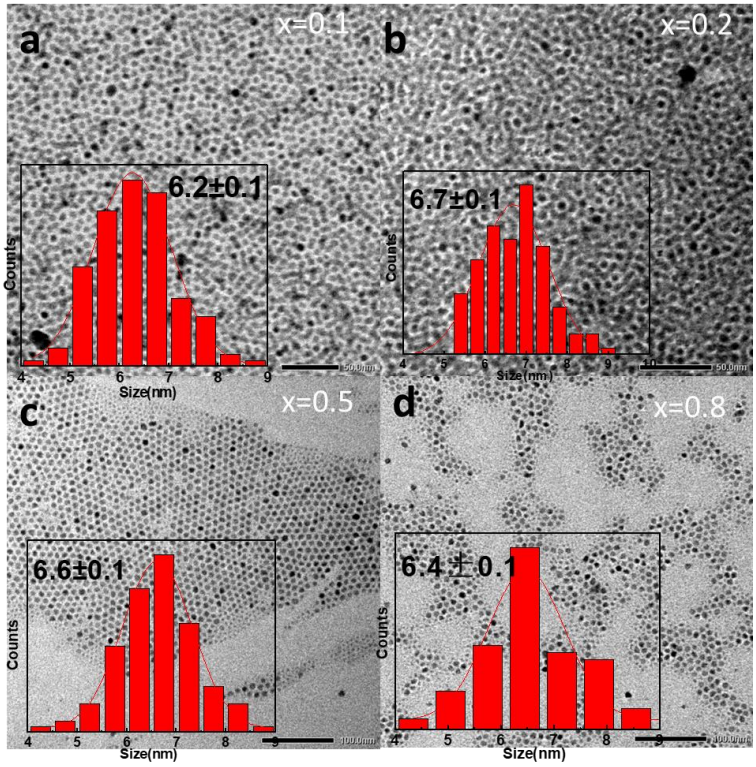

Figure S2.3. TEM images for the core $NaY_{0.9-x}Yb_{0.1}Nd_xF_4$ (x = 0.1, 0.2, 0.5, and 0.8) NPs. The inset shows the corresponding size distribution. The average size of the core $NaY_{0.9-x}Yb_{0.1}Nd_xF_4$ NPss is estimated to be about 6.2, 6.7, 6.6, and 6.4 nm for x = 0.1, 0.2, 0.5, and 0.8 while the average size for the corresponding core/shell structure is about 8.3, 10, 9.4, and 9 nm, respectively. This suggests a shell thickness of 1.1, 1.6, 1.4, and 1.3 nm for the $NaY_{0.9-x}Yb_{0.1}Nd_xF_4$ @CaF_2 core/shell NPs with x = 0.1, 0.2, 0.5, and 0.8, respectively. As a result, the thickness of the shell is about 1.1-1.6 nm for all the synthesized core/shell NPs, in good agreement with HAADDF STEM result (**Figure 1b**), while the core size remains almost identical with 6-7 nm for all doping rates.

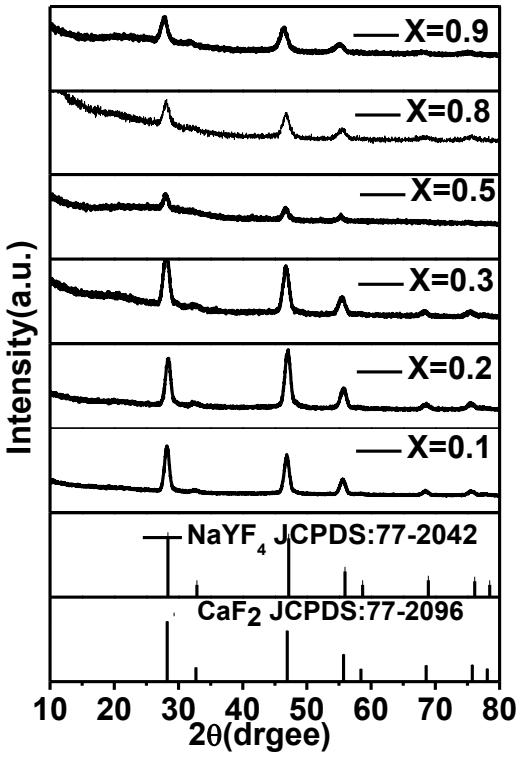

Figure S2.4. XRD patterns of $NaY_{0.9-x}Yb_{0.1}Nd_xF_4$@$CaF_2$ core/shell NPs with x = 0.1-0.9. The standard patterns of cubic $NaYF_4$ (JCPDS 77-2042) and CaF_2 (JCPDS: 77-2096) are included below for reference.

S3. Compositional analysis of $NaYF_4$:Yb,Nd @CaF_2 core/shell nanoparticles.

	Ca(ppm)	Na(ppm)	Nd(ppm)	Y(ppm)	Yb(ppm)	Nd(mmol%)	Yb(mmol%)
x = 0.3 y = 0.1	14.275	2.648	2.857	4.323	1.321	26%	10%
x = 0.1 y = 0.1	8.018	2.377	0.580	3.407	0.765	9%	10%
x = 0.2 y = 0.1	17.177	1.305	2.403	6.211	1.587	18%	10%
x = 0.5 y = 0.1	28.122	1.155	4.772	3.751	1.580	39%	11%
x = 0.8 y = 0.1	19.728	1.199	9.689	1.017	1.690	76%	11%
x = 0.9 y = 0.1	10.870	1.064	7.298	0.029	1.162	88%	11%

Table S3.1.- Results of the compositional analysis of $NaY_{0.9-x}Yb_yNd_xF_4@CaF_2$ employed in this work obtained by inductively coupled plasma–mass spectrometry (ICP).

S4. Lifetime curves obtained at 1340 nm.

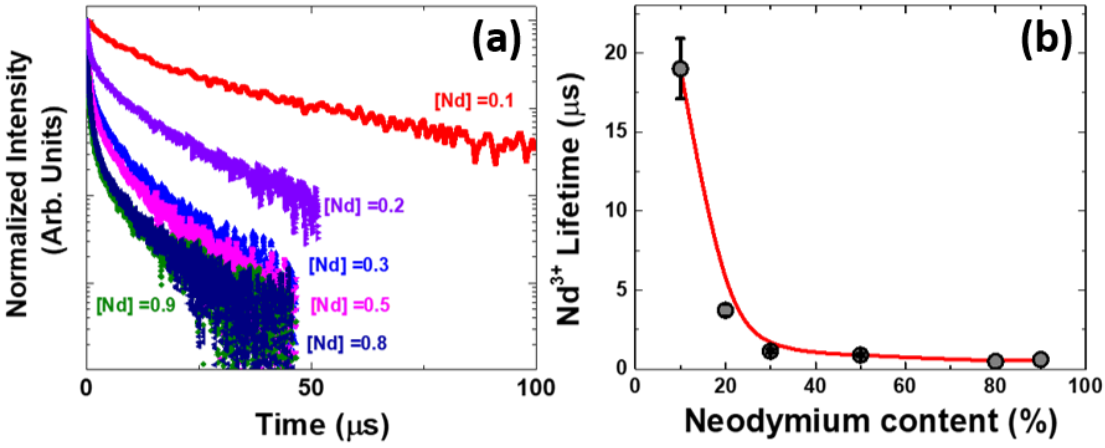

Figure S4.1 (a) Fluorescence decay curves obtained for the $NaYF_4$:Yb,Nd@CaF_2 core/shell NPs with six different Nd^{3+} doping levels. Excitation was performed at 808 nm and the emission wavelength was 1340 nm so that the registered emission is generated by transitions from the $^4F_{3/2}$ level of neodymium ions. **(b)** Concentration dependence of the 1340 nm (Nd^{3+}) luminescence lifetime of the NPs. Dots are experimental data obtained from **(a)** and line is a guide for the eyes.

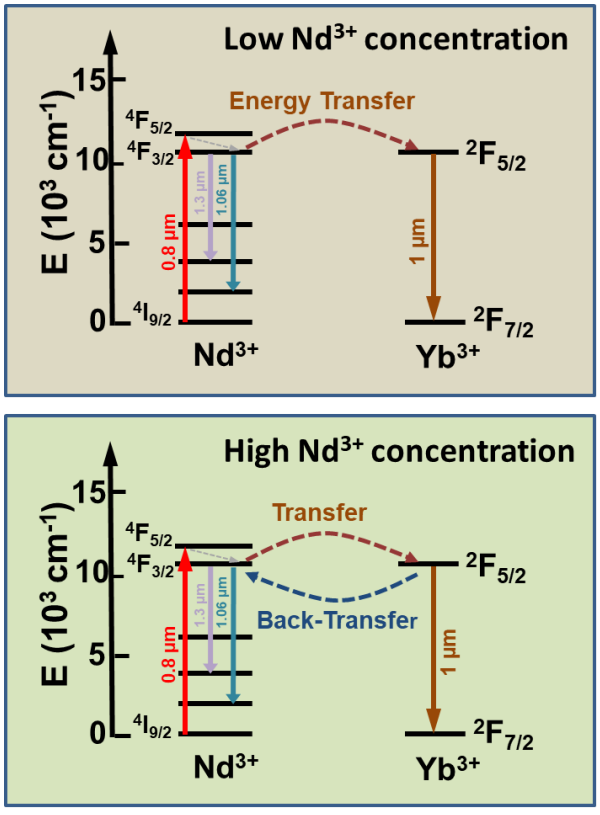

Figure S4.2. Schematic energy level diagram of neodymium and ytterbium ions. The different transitions are indicated for the cases of low and high neodymium concentration. Note the appearance of energy back transfer processes for high neodymium concentrations.

S5.- *Ex vivo* images.

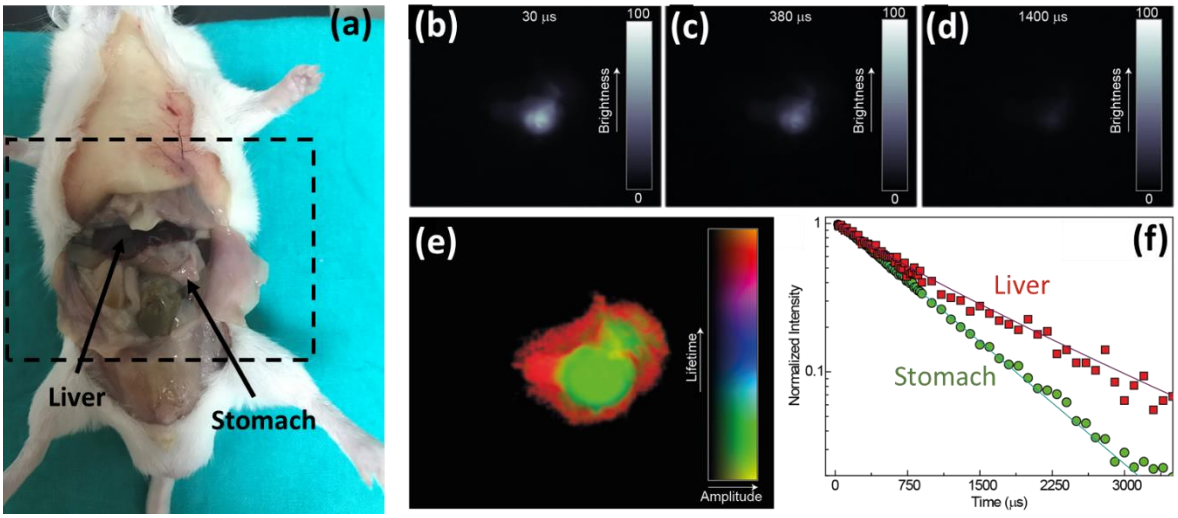

Figure S5.1. (a) Optical image of the euthanized mouse after oral and intravenous injection of NPs with Nd^{3+} concentrations of x = 0.3 and 0.2, respectively- The position of the stomach and the liver is indicated by arrows. **(b)**, **(c)** and **(d)** correspond to the fluorescence images obtained for different time delays between laser excitation and image acquisition. **(e)** *Ex vivo* lifetime image of the mouse shown in (a) denoting the clear location of the NPs administrated orally and intravenously. **(f)** Luminescence decay curves obtained in the stomach and the liver.

S6.- *In vivo* multiplexed images.

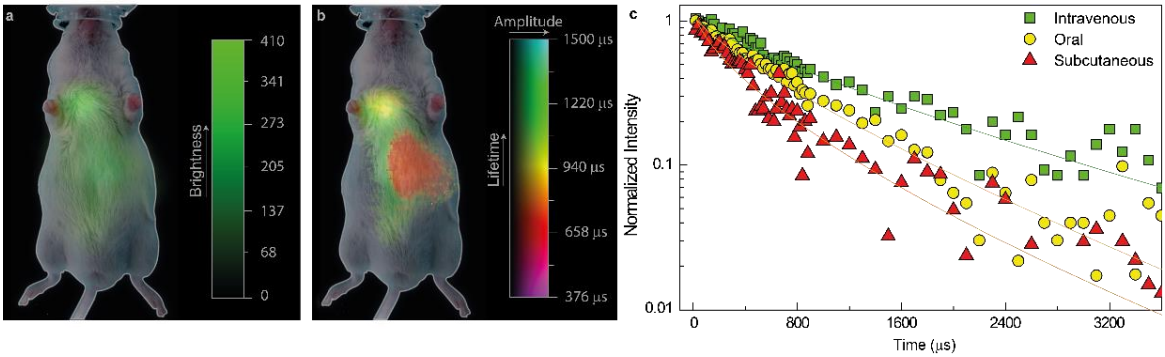

Figure S6.1. *In vivo* multiplexed lifetime imaging: **(a)** Intensity-based infrared image of a mouse after oral, subcutaneous and intravenous administration of $NaY_{0.9-x}Yb_{0.1}Nd_xF_4@CaF_2$ NPs with a Nd^{3+} content of x = 0.3, 0.2 and 0.5, respectively. **(b)** Lifetime-based image of same mouse as in (a). The different location of the three types of NPs can be observed. **(c)** Fluorescence decay curves obtained at three different locations corresponding to $NaYF_4$:Yb,Nd @CaF_2 core/shell NPs administrated orally, subcutaneously, and intravenously. Symbols are experimental data and solid lines are best exponential fits.

S7.- Concentration dependence of the emission spectra.

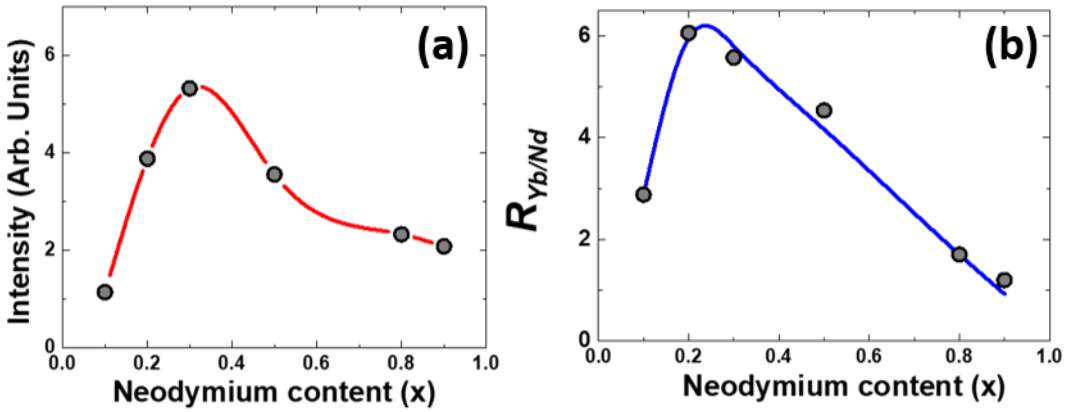

Figure S7.1. (a) Integrated (850-1500 nm) emission generated by colloidal solutions of the core/shell NPs as a function of the Nd^{3+} content. Dots are experimental data and solid line is a guide for the eyes. **(b).** The ratio between the emitted intensities at 980 nm (generated by ytterbium ions) and at 1340 nm (generated by neodymium ions) as a function of the neodymium content. The dots are experimental data and solid line is a guide for the eyes.

S8.- *In vivo* toxicity studies.

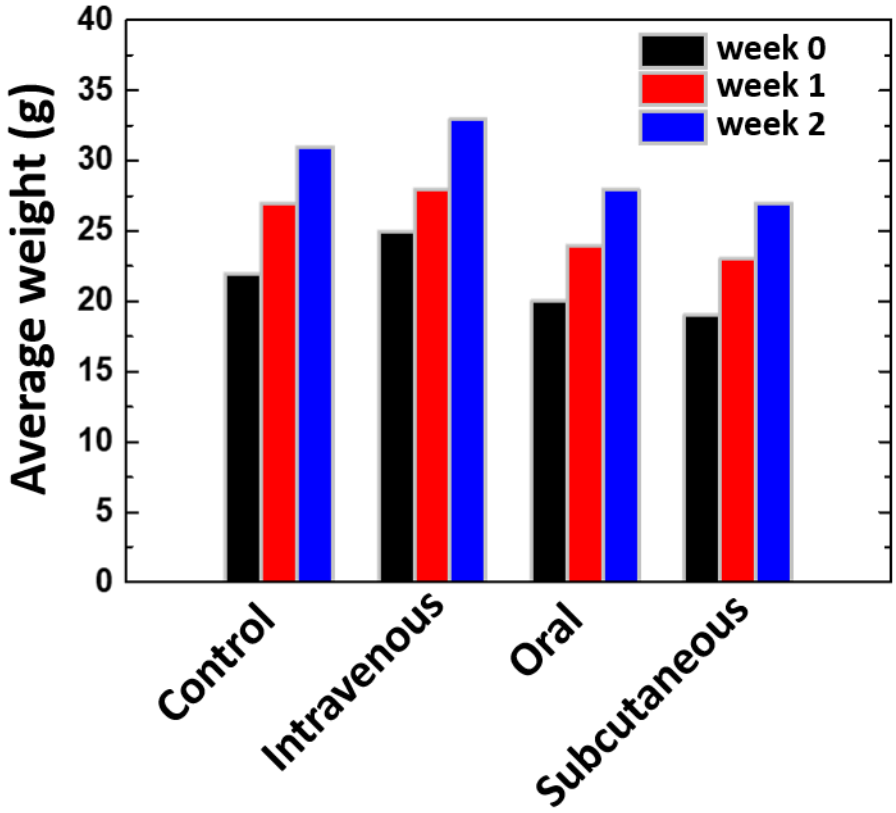

Figure S8.- Time evolution of the average weight of mice after oral (200 µL aqueous dispersion), subcutaneous (50 µL aqueous dispersion) and intravenous (100 µL dispersion in PBS) administration of $NaYF_4$:Yb,Nd@CaF_2 core/shell NPs at concentrations of 20 mg/mL. Results obtained for control mice are also included. No signs of toxicity are observed in any of the examined cases.

REFERENCES

1. Lee, K. C. B.; Siegel, J.; Webb, S. E. D.; Lévêque-Fort, S.; Cole, M. J.; Jones, R.; Dowling, K.; Lever, M. J.; French, P. M. W., Application of the Stretched Exponential Function to Fluorescence Lifetime Imaging. *Biophys. J. 81*, 1265-1274.
2. Siegel, J.; Lee, K. C. B.; Webb, S. E. D.; Leveque-Fort, S.; Cole, M. J.; Jones, R.; Dowling, K.; French, P. M. W.; Lever, M. J. In *Application of the Stretched Exponential Function to Fluorescence Lifetime Imaging of Biological Tissue*, European Conferences on Biomedical Optics, SPIE: 2001; p 9.
3. Laherrère, J.; Sornette, D., Stretched Exponential Distributions in Nature and Economy: "Fat Tails" with Characteristic Scales. *Eur. Phys. J. B* **1998,** *2*, 525-539.